Experimental investigation of QCM-derived sticking coefficients for use in molecular transport simulations

Lubos Brieda[a,b], Elana Helou[b], Tianxiang Zhao[b], Joseph Wang[b], Denisse Aranda[c], Vince Green[c], Syed Iqbal[c]

[a]Particle in Cell Consulting LLC, Westlake Village, CA 91362, USA
[b]University of Southern California, Los Angeles, CA 90090, USA
[c]Blue Origin, Kent, WA 98032, USA

ABSTRACT

This paper presents data from an experimental characterization of molecular transport in vacuum chambers. Specifically, our goal was to determine the applicability of a Quartz Crystal Microbalance (QCM)-derived sticking coefficients for modeling gray-body view factors. The testing was performed at Blue Origin and at USC, and consisted of performing a QCM thermogravimetric analysis (QTGA) to derive the sticking coefficient from a QCM with a direct line of sight to an outgassing sample. This sticking coefficient was then used in a numerical simulation of the chamber, which was used to compute deposition on a secondary QCM with no direct line of sight to the sample. The simulations were found to greatly under-predict the collection on the second QCM. This under-prediction is attributed to the sticking-coefficient based adhesion model reducing flux on each wall impact. In reality, the contaminant population is composed of a heterogeneous mixture of multiple chemical species. Lower vapor pressure gases collect on the first wall impact, while the remaining molecules continue to bounce around without additional sticking. A temperature-based sticking coefficient applies the reduction on each impacting, leading to an artificially low prediction for gray body deposition onto the final cold surface. For the two considered configurations, we found the model to underestimate the experimental measurements by a factor ranging from 7.2 to 1764.3.

Keywords: spacecraft contamination, vacuum environment, molecular transport

1. INTRODUCTION

Contamination transport analyses are routinely performed for science missions in order to predict the thickness of molecular film or the surface concentration of particulates after some prescribed mission duration. Alternatively, the analysis can be helpful in establishing the desired beginning of life (BOL) cleanliness level needed to meet mission requirements. These analysis involve determining what fraction of mass generated by source elements reaches, and deposits, to target regions of interest. The primary challenge in simulating contamination transport arises from the ambiguity in capturing the re-emission from secondary surfaces. Upon contacting a surface, molecules temporarily adhere to it, until due to random vibrational effects, they "shake themselves loose". The time spent on surface is known as the *residence time*,

$$\tau_r = \tau_0 \exp\left(\frac{E_a}{RT}\right) \tag{1}$$

where τ_0 is assumed to be $\approx 10^{-13}$ s. The term E_a is called the *activation energy*, and is given by Tribble[1] to be in 1 to 10 kCal/mol range for a surface desorption process. The remaining terms are the surface temperature T and the universal gas constant $R \approx 1.987$ cal/mol/K. One take away from this relationship is that residence time scales with the surface temperature T. For $E_a = 8$ kCal/mol and $T = 300$ K, Equation 1 evaluates to 6.7×10^{-8} seconds, which is essentially negligible. This molecule can be assumed to not stick. On the other hand, the residence time increases to almost 8.5 hours once the temperature drops to 100 K. Molecule impacting this surface can be assumed to be permanently stuck.

Corresponding author: lubos.brieda@particleincell.com.

Unfortunately, Equation 1 is of a limited practical use. First, it does not take into account the already adhered molecular film. One can imagine a difference in chemical compatibility between different kinds of reactants. Secondly, the molecular contaminant population encountered in spacecraft testing is a "soup" of a multitude of different chemical species, each with their own activation energies. There doesn't exist any practical way of estimating this species distribution or their appropriate activation energies. Even devices like the Residual Gas Analyzer (RGA) seem to be only of limited use. For this reason, it is customary to treat the molecular contaminants as if made of a single chemical "VCM" (volatile condensable material) species and use a *sticking coefficient* to control the redistribution. While for a conservative assessment one could make all non-sensitive surfaces perfect re-emitters ($c_{stick} = 0$) and all sensitive surfaces perfect sinks ($c_{stick} = 1.0$), a more realistic assessment can be made by letting $c_{stick} = c_{stick}(T)$ be a gas material property. Conceptually, this temperature dependent sticking coefficient can be obtained experimentally using Temperature-controlled Quartz Crystal Microbalance (TQCM). These devices are the primary instruments for monitoring outgassing in bakeouts or thermal vacuum tests. The device consists of a crystal exposed to the vacuum environment. The temperature of the crystal can be varied from around -40 °C below the QCM body to about 80 ° C. The amount of mass deposited on the crystal affects its vibrational frequency. The frequency difference between the exposed and an internal reference crystal can then be correlated to the amount of collected mass through a linear scaling law. The crystal needs to be periodically baked off to remove the deposited material. This is done by warming up the crystal to the 80 ° (or so) upper limit temperature. Instead of doing this warm up as quickly as possible, we can let the temperature increase at a constant rate, such as 3 °C/min. The attained non-uniform mass removal rate can then be normalized to yield the sticking coefficient. This approach of obtaining an insight into the molecular composition of the collected contaminants is called a QCM ThermoGravimetric Analysis (QTGA or TGA for short).

The goal of the research study described in this paper was to determine whether a TGA-based sticking coefficient actually works in practice. Obtaining experimental data usable for contamination transport validation studies is incredibly difficult. In our experience, spacecraft missions tend not include a budget line item for basic research into the physics of contamination transport. Any experimental data is then limited to measurements obtained in support of spacecraft thermal vacuum testing. This introduces two challenges. First, the collected data may fall under export control regulations due to the presence of flight hardware. Secondary, this data is not particularly useful. Even "detailed" engineering CAD drawings do not capture all aspects of the spacecraft configuration. As an example, the blanket design and vent paths may not be included at all. Chamber facilities also need to be fitted with various support mechanical ground support equipment (MGSE) such as scaffolding, non-flight harnessing, heaters, and instruments. These features area also not likely to be included in the CAD model. Therefore, we envisioned a dedicated experimental setup consisting of two QCMs placed in a vacuum chamber along with an outgassing sample and the necessary support structures. One QCM was oriented to have a direct line of sight to the sample. The TGA from this QCM is used to derive the sticking coefficient. Another QCM is placed in a secondary location facing the wall so that any molecules reaching it need to undergo a re-emission. If the sample is heated to temperature above the chamber walls, we can expect the molecular population to contain a component that requires these high temperatures to desorb. In other words, this population will condense on the chamber walls. Thus, we should expect the second QCM to: a) report a lower deposition rate due to a loss of some contaminant to the walls, and b) have a TGA that is identical to that of QCM 1 but with the high temperature component cut off. As will be reported below, the reality ended up being somewhat more complicated. We begin the paper by describing the numerical model used for contamination transport modeling. We then describe the experiment and introduce the data. We also include plots from simulation results. The testing was performed at two locations: a front-loading vacuum chamber at Blue Origin's Kent, WA facility and a smaller top-loading chamber at USC's Laboratory for Exploration and Astronautical Physics (LEAP). The paper is concluded with a summary of future work.

2. MOLECULAR TRANSPORT MODELING OVERVIEW

Conceptually, the temporal variation in deposited contaminant mass on some surface element i is given by

$$\dot{m}_i(t) = \sum_{j \neq i} \left[\nu_j(t) + \gamma_j(t)\right] A_j F_{ji} - \nu_i(t) \quad , i = 1, \ldots, N \tag{2}$$

where ν is the mass desorption rate (kg/s), γ is the surface outgassing rate (kg/s), A is the surface area (m^2), and F_{ji} is the area-normalized black-body "form factor". It specifies the fraction of molecules emitted from element j that reach element i without re-emission from a secondary surface. The time evolution of mass on element i is due to the outgassed and desorbed mass arriving from all other elements minus the mass desorbing from it. The time variation of surface mass can then be estimated by numerically integrating Equation 2 using a method such as the first order Forward Euler,

$$m_i(t + \Delta t) = m_i(t) + \dot{m}_i \Delta t \tag{3}$$

The F_{ji} form factor matrix has been historically computed using thermal radiation codes, such as Thermal Desktop or the Thermal Synthesizer System (TSS). This is applicable since in the absence of collisions in the low density space environment, molecules move in straight lines, just like photons, at least between surfaces. Therefore, the fraction of radiation reaching surface j from element i provides the black body view factor F_{ji} needed for the contamination analysis. The thermal codes perform this calculation by launching a large number of rays from each surface element and determining which other surface element the rays intersect, unless they are lost to space. The resulting large and dense matrix would then be ingested by some custom code that performs the integration in Equation 3.

Several years ago, we have demonstrated an alternative approach in our Contamination Transport Simulation Program (CTSP).[2,3] CTSP simulates molecular transport using an approach derived from the Direct Simulation Monte Carlo (DSMC)[4] and Particle in Cell (PIC)[5] algorithms commonly used by the rarefied gas and rarefied plasma physics communities. Unlike in the legacy radiation based approaches, CTSP concurrently simulates the entire gas population, which makes it possible to include molecular collisions when needed. This allows the code to compute volumetric data, such as contaminant plume partial pressure, temperature, or streaming velocity. The code also directly takes into account re-emission. On each surface impact, some specified surface handler is used to determine whether the incident molecules should "stick" or whether it should be reflected back to the gas domain. Simulations begin with the domain free of any gas. The specified geometry is then loaded from a triangular and/or quadrilateral surface mesh file. The simulation then runs for a user specified number of time steps. New particles are continuously injected from all source elements. During each time step, each particle traverses a small distance $\Delta\vec{x} = \vec{v}\Delta t$. This line segment is checked for surface impacts by performing line-triangle checks against the local elements. If an impact occurs, a surface handler uses material properties, surface temperature, as well as user-specified adsorption model to determine whether the particle sticks or is re-emitted. After some number of time steps, the simulation reaches a steady state at which the number of new injected particles matches the loss at the domain boundaries. The simulation then continues for more steps to smooth out the results.

2.1 Sticking Coefficient

The surface handler mentioned previously can take many forms. For instance, in a prior work involving modeling ice build up on the James Webb Space Telescope,[6] we used the saturation vapor pressure of water to model icing. Other approaches involve computing residence time based on a specified activation energy. However, it is our experience that the most commonly applied approach involves assigning to each flying material a temperature-dependent sticking coefficient. The temperature of the impacted surface is then used to evaluate the actual c_{stick}. It is used in conjunction with another random number to stochastically determine whether the molecule sticks or not. Alternatively, the sticking coefficient can be used to split off the macroparticle into a fragment that remains stuck to the wall and the fraction that re-emits.

This is where the difficulty lies. Materials used in a spacecraft construction are characterized using tests such as ASTM-E-595 or ASTM-E-1559. The sample is placed in a vacuum chamber and is heated to some assigned temperature. One or more QCMs held at a prescribed temperature measures the deposition rate. In the case of ASTE-E-595, only a single QCM held at 25 °C is used. The sample is nominally heated to 125 °C (399.15 K). By comparing mass before and post test we can determine the total amount of desorbed mass, and can also estimate the fraction of this mass corresponding to water. The ASTM-E-1559 test uses 3 QCMs set to $\leq$ 90 K, 160 K and 298 K. The coldest QCM allows us to directly measure water. These characterization tests provide only the minimum information relevant to determining surface sticking behavior. QCMs however afford us the possibility

of estimating the sticking behavior by performing a QCM-based Thermogravimetric Analysis (QTGA). This is the community-used term for warming up the QCM crystal at a fixed rate, and using the frequency rate of change to determine at which temperatures material tends to desorb. This information could be used to create a spectrum of different material species of varying activation energies. Alternatively, the normalized amount of mass remaining on the crystal at a given temperature can be used to generate a temperature-varying sticking coefficient.

3. BLUE ORIGIN TESTING

3.1 Experiment Setup

The goal of this work was to test the validity of this QTGA-derived sticking coefficient for modeling gray-body molecular transport. To do so, we have devised what was initially believed to be a simple experiment. A test article is placed in a vacuum chamber and is attached to a heater. We then position one QCM so that it has a direct line of sight to the sample. This QCM is used to obtain the steady-state outgassing characteristics of the test sample. This characterization includes performing the TGA to obtain the $c_{stick}(T)$ curve for the contaminant gas. Since the sample is heated to a temperature above the chamber walls, we expect that the contaminant population will contain some component that condenses at the ambient wall temperature. A second QCM is oriented such that it does not have a line of sight to the sample. Specifically, this QCM is placed near and facing one of the walls. Any molecules reaching it have to undergo wall collisions. The deposition rate onto this QCM is expected to be reduced by the loss of the high temperature component. A TGA performed using the material condensed onto the second QCM should show species identical to what was observed on QCM 1, except that there should be a clear cut off around the wall temperature.

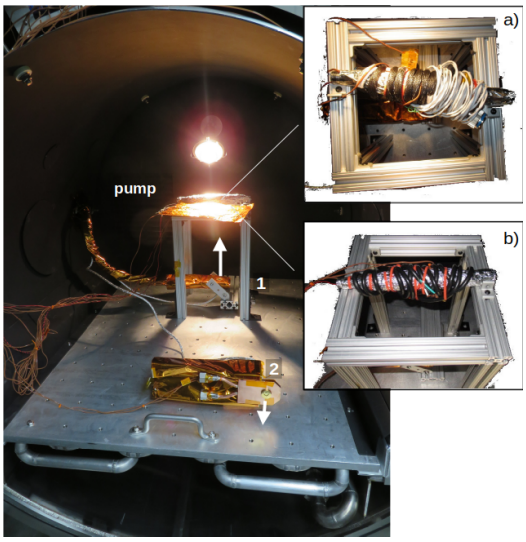

Figure 1. Experimental setup utilized at Blue Origin. The insets illustrate the two test samples: a) flight harness, b) unbaked electrical cord.

To confirm this hypothesis, we performed two parallel studies, with one utilizing a vacuum chamber at Blue Origin, and the second using a small top-loader chamber at USC's LEAP lab. Testing at Blue Origin afforded us the option of obtaining data from an actual flight support facility with equipment beyond that available at the university setting. We utilized a 5' x 5' chamber pumped with a single turbopump, providing up to 5.0×10^{-7} Torr base pressure. Figure 1 shows the experimental setup. It consisted of a test sample placed onto a 18.5" tall T-slot aluminum support structure, which itself was placed towards the back chamber wall. A QCM Research Mark 26-1 QCM (QCM 1) was centered below the sample, with a line of sight towards the sample. A second QCM Research Mark 26-1 QCM (QCM 2) was placed on the platen close to the front door. This QCM was oriented such that its line of sight is limited to the door.

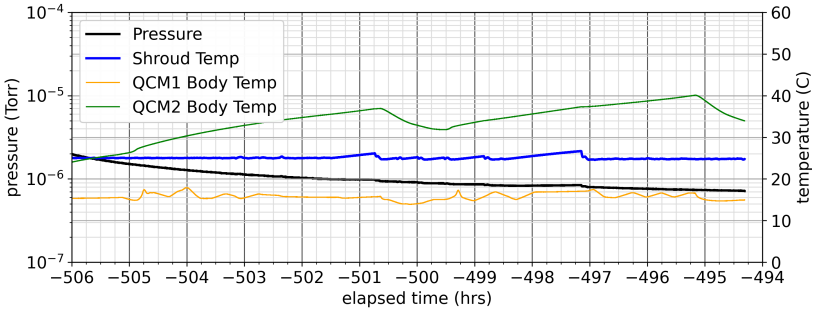

(a) Chamber Telemetry

Figure 2. Baseline empty chamber readouts of chamber pressure and some relevant temperatures

3.2 Baseline

Prior to testing, the baseline cleanliness of the chamber was characterized. This run was also used as a checkout of the QCMs and the heaters. Figure 2 plots the chamber telemetry from this run. The time on the horizontal axis corresponds to the number of hours since the beginning of the test described in the next section, and hence this pre-test data shows negative values. The baseline chamber pressure, in black, can be seen to hover around 10^{-6} Torr. The orange and green curve plot the body temperature of the two QCMs. The higher value, and the decreased stability, of QCM 2 temperature arises from the lack of active cooling due to an unavailability of plumbing lines.

Figure 3 then visualizes the data collected on the QCMs. Data for QCM 1 is shown in black, while the blue line plots the trace for the wall-facing QCM 2. Outgassing was sampled between hours -505 and -501 with QCM 1 set to -55 °C while QCM 2 was set to -20 °C. A TGA was subsequently performed by warming up the crystal at uniform rate of 3 °C/min. In the bottom half of the picture we see the numerically derived frequency rate. These plots were generated with a custom Python script that loads the provided chamber telemetry, RGA, and QCM data files, and perform the appropriate reduction. Frequency rate was computed by performing numerical differentiation using central differencing. To reduce noise, a 30-item long stencil was used. In other words,

$$\left(\frac{df}{dt}\right)_i = \frac{f_{i+30} - f_{i-30}}{t_{i+30} - t_{i-30}} \tag{4}$$

Since QCM data was sampled at a one second interval, this differencing averages the frequency over a one minute interval. Sensitivity study was performed with different window sizes to verify that this averaging does not introduce non-physical artifacts. The deposition rate on the colder QCM 1 was about 1.7× greater than the deposition rate on the warmer QCM 2, which was approximately 140 Hz/hr at the conclusion of the characterization run.

Figure 4 visualizes the two TGAs performed with the empty chamber. The darker lines plots the rate of change of frequency in respect to temperature, df/dT. The lighter lines show the absolute value of the second derivative, $|d^2f/dT^2$. The zero values (roots) indicate temperatures where the df/dT plot levels off, thus indicting transitions between different molecular constituents. These plots come from another Python script that performs this numerical differentiation over prescribed time intervals. This script also computes the sticking coefficient, described below, by computing the normalized mass lost as a function of temperature. Looking at the darker lines, we can notice some difference in the -20 to +10 ° C region, likely arising from the difference in collection temperatures. However, both QCMs indicate a strong peak around 25 °C which must be due to outgassing from chamber walls and other MGSE. While this population should be included in the subsequent numerical simulations, doing so remains as future work.

3.3 View Factor Modeling

In parallel with the experimental characterization at BO, the PIC-C/USC team obtained dimensions of the vacuum chamber and used them to create a CAD model. The meshed version was subsequently used for CTSP

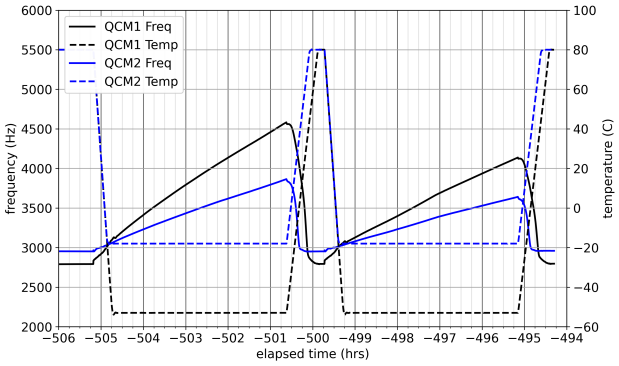

(a) Crystal frequency and temperate

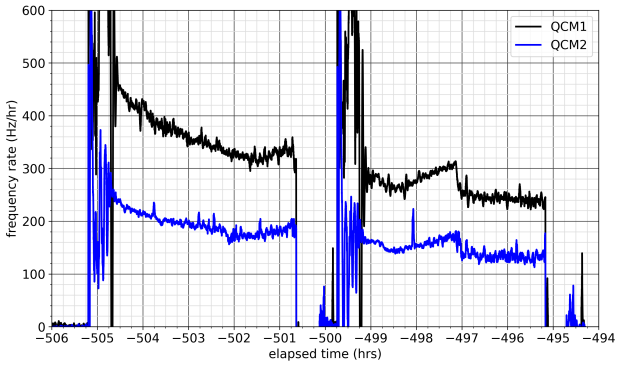

(b) QCM rate

Figure 3. QCM frequency and temperature (top) and the corresponding rate (bottom) for the baseline empty-chamber characterization.

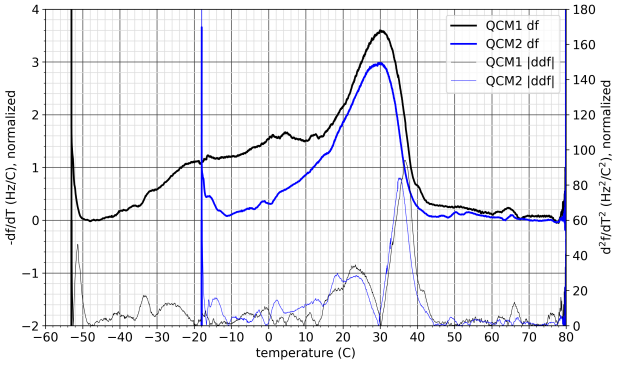

(a) -500.65 to -499.85

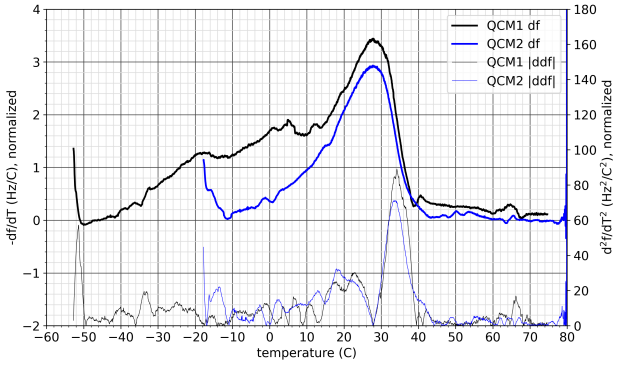

(b) -495.15 to -494.44

Figure 4. Baseline empty chamber TGA.

simulations. Numerical modeling allows us to compute the expected maximum view factor between the sample and the two QCMs. This view factor corresponds to the warm-wall configuration in which nothing sticks to the walls. We set a zero sticking coefficient on all surfaces, which included the chamber thermal shroud, the chamber walls, the test fixture, as well as the QCM bodies. The exception were the pump and the two QCM crystals, which were assigned a 100% sticking. Nominally making the pump inlet a sink will over-predict the effective pump area. But in this chamber, the pump inlet is placed behind fixed louvers. Molecules leaving the thermal shroud enclosure become trapped in the cavity between the shroud and will eventually reach the pump.

The numerically computed molecular number density is plotted in Figure 5. Molecules were injected from the cylindrical "cable bundle" placed on top of the support structure. While we can notice a slightly elevated number density in the vicinity of the source, the density is otherwise fairly uniform throughout the enclosure. The same is true for the population between the chamber wall and the thermal shroud, although the density here is decreased by about an order of magnitude. This is expected, since in a warm-wall configuration, molecules simply bounce around the chamber leading to uniform pressure. CTSP also keeps track of the deposited mass on different surface components. This trend is shown in Figure 5(b). After 90,000 time steps, mass deposited on the three sinks is

zone	mass	ratio
Pump	4.0864×10^{-12}	0.9611
QCM 1	8.3075×10^{-14}	0.0195
QCM 2	8.245×10^{-14}	0.0194

The actual values for the deposited mass are not relevant since we used an arbitrary injection flux on the

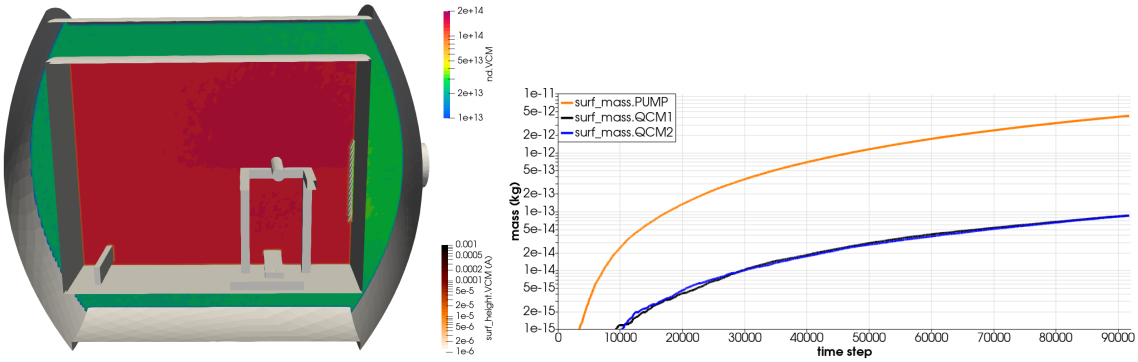

(a) number density (b) deposited mass

Figure 5. Numerical simulation used to compute warm-wall QCM view factors.

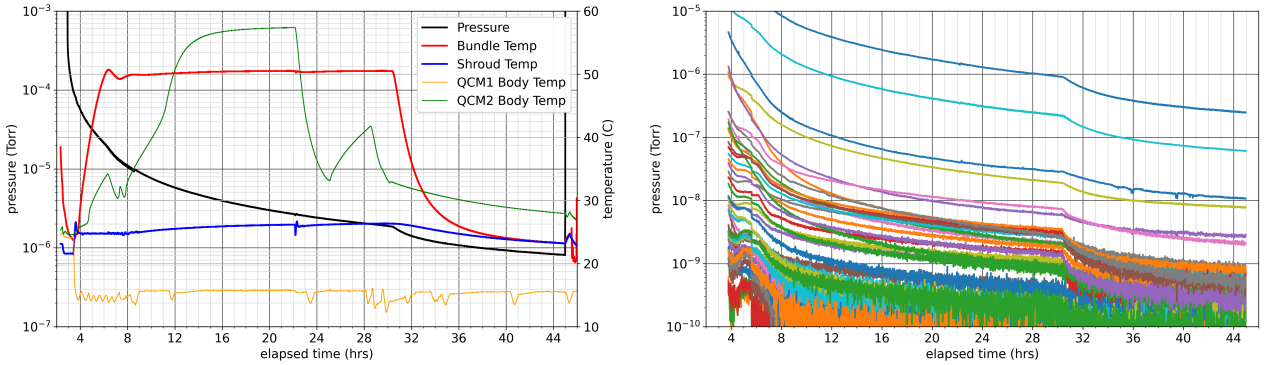

(a) Chamber Telemetry (b) RGA

Figure 6. Pre-baked flight harness chamber pressure and thermocouple data (a), and RGA partial pressures (b).

source. Instead, of interest is the ratio column. While we can see that the majority of the emitted mass is indeed collected by the pump, we also see that the two QCMs have essentially identical viewfactors to the sample. This is despite QCM 1 facing the sample directly, while QCM 2 is looking at the wall and has no direct line of sight to the sample. This perhaps non-intuitive finding arises from the complete re-emission on the walls.

3.4 Flight Harness

In late January 2022, the PIC-C/USC traveled to Blue Origin's Kent, WA facility to participate in data collection. The first attempt utilized a pre-baked flight harness, shown by the (a) inset in 1. Chamber telemetry from this run is plotted in Figure 6. The wire bundle heaters were activated about 4 hours after pump down, with the harness remaining at 50 ° C for 24 hours. Chamber pressure is seen to decay from around 10^{-5} Torr at hour 4 to 2×10^{-6} Torr at hour 30. Deactivating the heater led to a subsequent pressure drop down to about 9×10^{-7} Torr. The second plot shows the temporal variation in RGA partial pressures for molecular masses 1 through 100. This graph is not annotated due to difficulties in including a legend consisting of 100 entries. The main takeaway is that there do not appear to be any individual dominant species that track with the wire bundle temperature. Instead, the entire spectrum seems to respond mostly in unison. This finding was quite unexpected as we envisioned the RGA trace allowing us to limit the contaminant population to a small number of chemical species or hydrocarbon fragments.

In the chamber telemetry data, we can also observe large variation in QCM 2 body temperatures. Only QCM 1 was actively cooled due to a lack of a secondary plumbing line. This lack of cooling is clearly apparent from the green line. In fact, the temperature on QCM 2 exceeded that of the test article as it reached about 55 °C at hour 16. This led to the QCM overheating, and being unable to maintain the prescribed -20 °C crystal set point. This overheat happened overnight and is clearly visible in the QCM data in Figure 7. Upon coming to

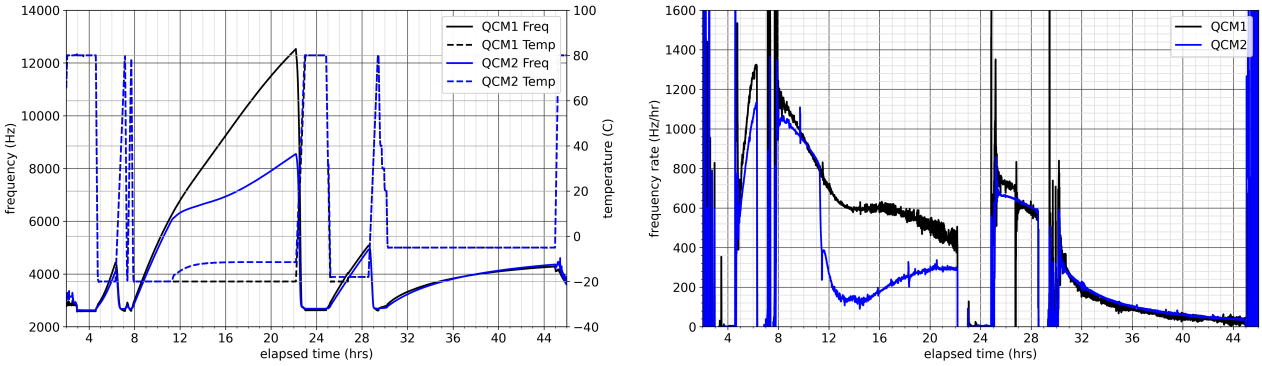

(a) QCM data (b) QCM rate

Figure 7. QCM measurements for the pre-baked flight harness.

the lab the next day, we performed a TGA and allowed the QCM 2 body to cool off. We then performed a reduced collection lasting only 4 hours (between hours 25 and 29), which was followed by a TGA. Subsequently we performed a longer data collection at a warmer crystal temperature (to prevent the overheat). It was also followed by a TGA, but this TGA was inconclusive. The QCM deposition rate decayed from 1200 Hz/hr at hour 8 to 600 Hz/hr by hour 28. With the harness heater switched off, deposition rate decreased to about 40 Hz/hr, but this was collected with a crystal set to -5 °C.

One interesting observation we can make from Figure 7(a) is that prior to the overheat, the two QCM rates are almost identical. This agrees with our warm-wall numerical modeling in Section 3.3. However, the TGAs are not as clear cut as anticipated. The TGAs are plotted in Figure 8. They correspond to a warm up rate of 2 °C/min (with some later TGAs used a slightly faster rate of 3 °C/min). Only the plots in (a) and (d) are directly comparable. The view in (b) is a "blank" obtained by performing a second TGA after the first one. It can be used to account for the thermal variation of the crystal and also to correct for the incoming flux, but this remains as future work. The plot in (c) corresponds to different initial crystal temperatures due to the overheat. What is noticeable is that the spectra are quite broad and also exceed past the chamber wall temperature of 25 °C. In fact, the TGAs show desorption up to around 40 °C. This is a very interesting finding that requires future work. It appears to confirm that surface adsorption is not a binary stick/does not stick process and molecular species that outgassed at temperature above ambient still have a sufficiently short residence time to adhere to the walls temporarily.

Figure 9 visualizes the "effective" sticking coefficient obtained from these TGAs. Specifically, we plot, on the log scale, the cumulative fraction of mass remaining as a function of temperature. The dashed line is the trace for the wall-facing QCM 2. Our initial hypothesis was that the two TGA sets will demonstrate comparable trends, however, the component corresponding to temperatures above chamber walls will be absent in data from QCM 2. This is mostly the case, especially when considering the curves plotted in blue from a latter point in the test. However, as alluded to above, this separation does not become significant until around 5-10 °C above the wall temperature. At the wall temperature, the two sticking coefficients are still almost identical.

The data shown in Figure 9 was used to generate the tabulated sticking coefficient for a CTSP simulation. Specifically, from QCM 1 data, we have:

```
c_stick:[1.00@253.0, 1.00@258.0, 0.99@263.0, 0.97@268.0, 0.92@273.0, 0.83@278.0,
         0.70@283.0, 0.55@288.0, 0.38@293.0, 0.24@298.0, 0.12@303.0, 0.05@308.0,
         0.04@313.0, 0.03@318.0, 0.03@323.0, 0.02@328.0, 0.02@333.0]
```

This data is shown in the syntax used by the CTSP input file, which lists the coefficient as a list of value-temperature tuples. Considering the 25 °C = 298 K wall temperature, about 24% of material emitted from the harness is expected to stick to the walls. This disagrees with the measurements in Figure 7, which clearly shows

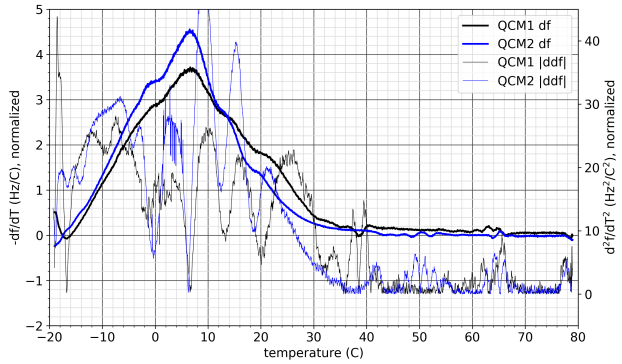

(a) 6.33 to 7.15

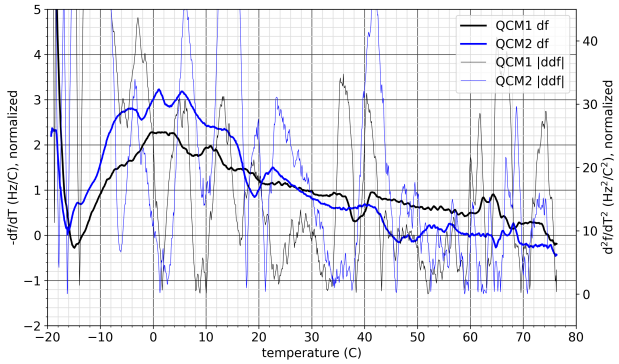

(b) 7.38 to 7.70 (blank)

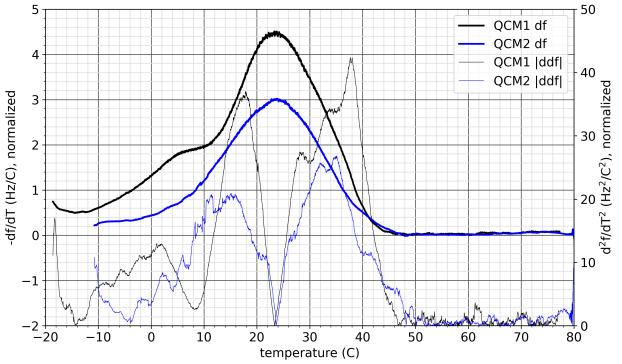

(c) 22.20 to 23.00

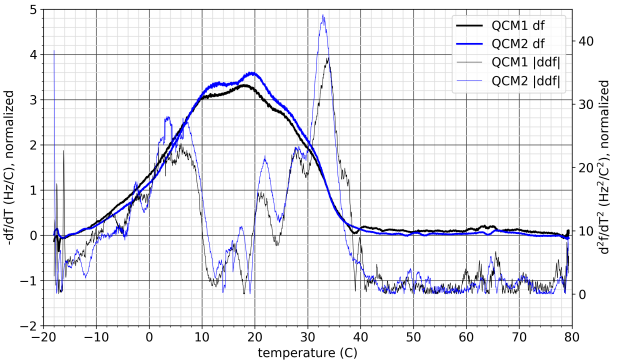

(d) 28.57 to 29.39

Figure 8. TGAs for prebaked electrical harness.

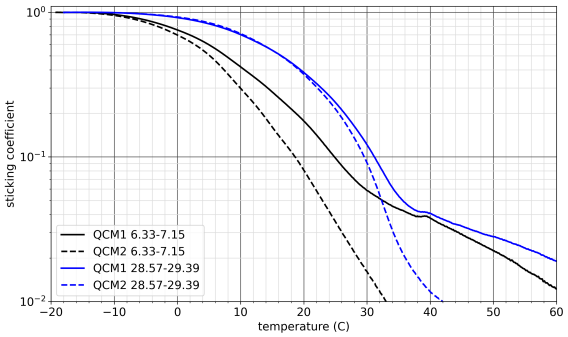

Figure 9. Sticking coefficient for the pre-baked harness, computed by considering the cumulative amount of mass lost during a TGA.

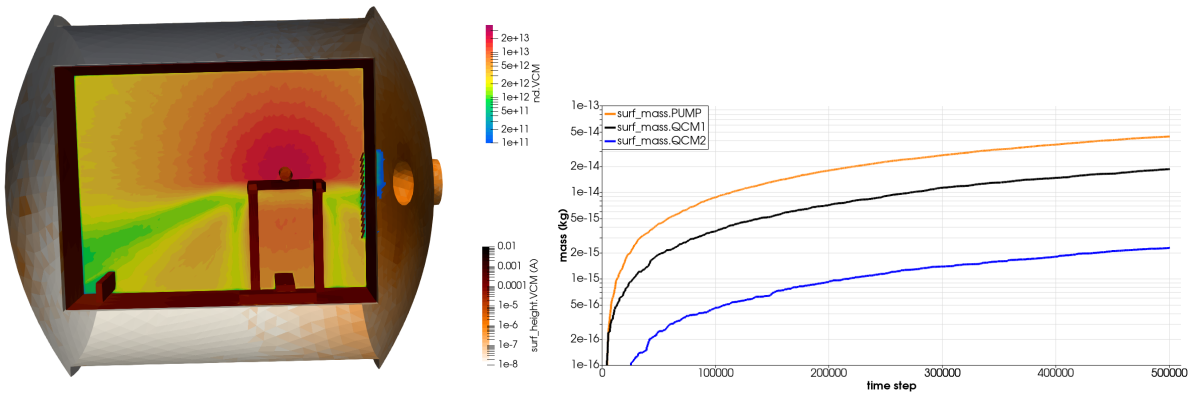

(a) number density (b) deposited mass

Figure 10. Numerical simulation using pre-baked harness sticking coefficients.

almost identical deposition rates on the two crystals. It appears the QTGA-based sticking coefficient is not as straightforward to apply as anticipated.

We next ran a simulation using the tabulated coefficient from above. Plots from this run are shown in Figure 10. After 500,000 time steps, the masses collected on the two numerical QCMs are 1.85×10^{-14} and 2.26×10^{-15}. Again, the actual values of mass are irrelevant since an arbitrary injection mass flux was used on the source. These results should only be compared qualitatively. The actual amount of deposited mass, and the actual gas number density, are both functions of the sample outgassing flux. We did not try to determine a physical value that would reproduce QCM 1 deposition rates from the experiment. Due to the implied free-molecular flow regime, the molecular pressure has no impact on gas dynamics. Of interest are the rates between the two crystals. Specifically, about 8.22× more mass collects on QCM 1 than QCM 2. The discrepancy between this ratio and the sticking coefficient at the wall temperature (and what is actually measured on QCM 2) is that CTSP (and many other similar codes) treat the contaminant as a single species of a variable sticking. Upon a wall impact, 24% of the incident mass is lost the wall and the remaining 76% is re-emitted. The molecule do not have any memory of past impact and thus a similar reduction happens on the second wall impact. Given that it may take multiple bounces for a molecule to reach QCM 2 crystal, the mass reaching it is greatly reduced by this exponential decay. Mathematically, the remaining mass after k wall collisions is 0.76^k. The predicted mass ratio thus corresponds to molecules undergoing roughly 7.7 wall collisions to reach QCM 2, which seems reasonable.

For the sake of completion, we also ran a simulation with an artificially increased cutoff at the ambient wall temperature,

```
c_stick:[1.00@253.0,1.0@290.0, 0.05@295.0, 0.02@333.0]
```

Results from this simulation are shown in Figure 11. As expected, the deposition rates on the two QCMs are now closer to each other. After 130,000 time steps (the extent of the simulation completion as of this report writing), the two masses were 1.5×10^{-14} and 9.3×10^{-15} respectively, for a ratio of 1.61. Utilizing 95% re-emission at the wall temperature, we see that this drop off corresponds to 9.3 wall impacts on average to reach the QCM 2. This is comparable to the finding in the previous paragraph, with the difference possibly arising from the smaller number of sampled time steps. Figure 12 provides two other visualizations of the simulation results. The shading on the surfaces corresponds to the amount of deposited material. While we can see shadowing by the test fixture and the QCM 2 body, the fact that there is a finite molecular density in this shadowed region implies that molecules re-emit from the walls.

3.5 Electrical Cord

Reviewing the TGAs for the pre-baked harness, we noticed a lack of a significant population at temperatures above the chamber walls. It is this population that we wanted to demonstrate as being lost between the two

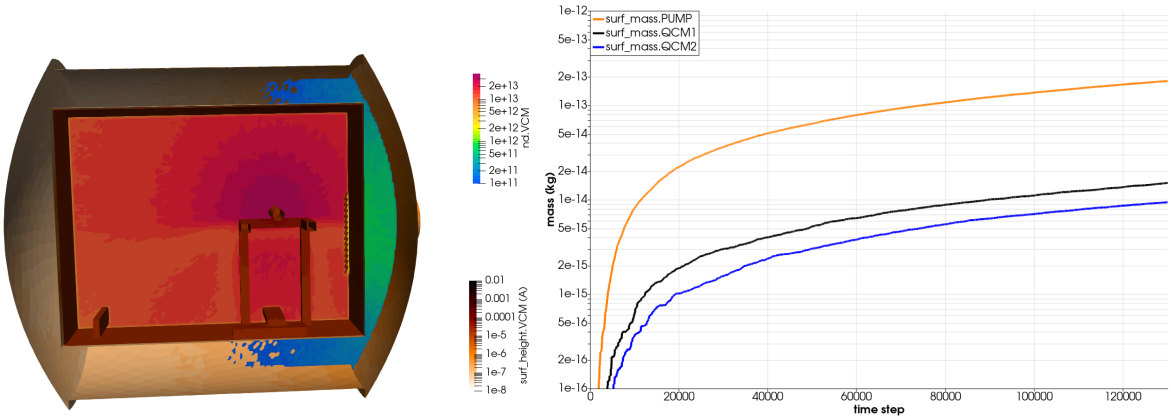

(a) number density (b) deposited mass

Figure 11. Numerical simulation using a prescribed c_{stick} with a cut off near ambient wall temperature.

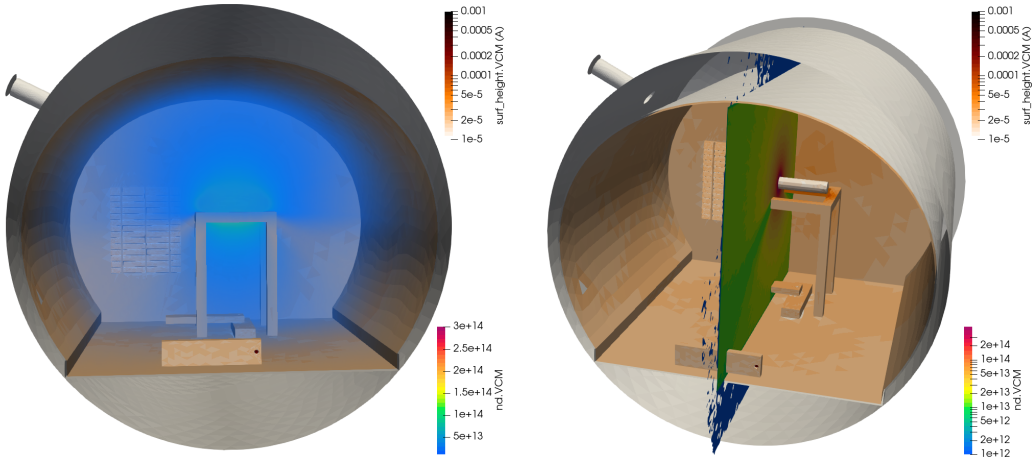

(a) view 1 (b) view 2

Figure 12. Additional views of numerical results.

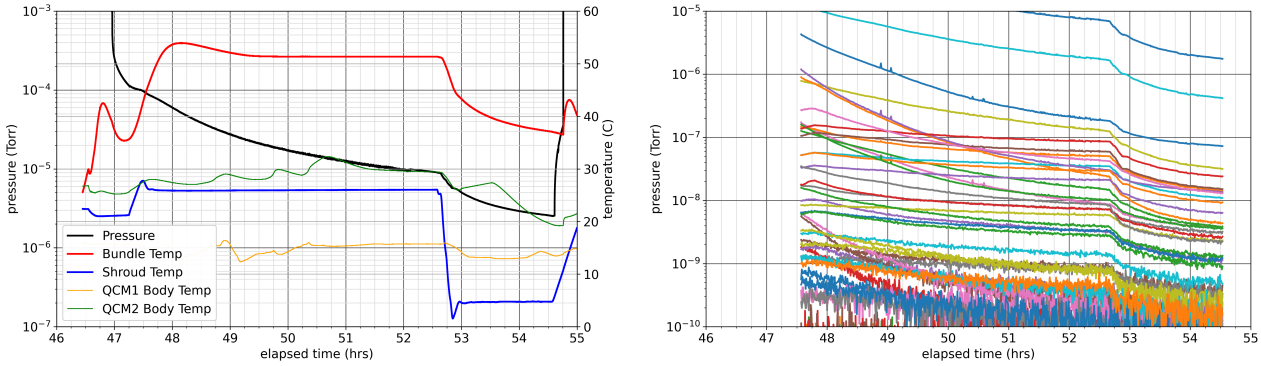

(a) Chamber Telemetry (b) RGA

Figure 13. Unbaked cable readouts of chamber pressure and thermocouple (a), and RGA pressures (b).

sensors. As such, we repeated the experiment using an unbaked electrical cable. It is shown by the inset (b) in Figure 1. The corresponding chamber telemetry is in Figure 13. The blue curve is again the chamber shroud, which can be seen to drop to 5 °C around hour 52.75. This drop was used to force the wall to become a collector to obtain a greater difference between the two QCMs. One observation we can make right away is that the chamber pressure is increased by about an order of magnitude from when the flight harness was used. This increase indicates a higher outgassing rate. Yet once again, we do not observe the presence of unique chemical species associated with the cable outgassing in the RGA time history. This finding is quite curious as we expected there to be only a handful of chemicals to be preferentially released as the cable is warmed up. Instead, the outgassing appears to be broad-spectrum. Performing a more detailed review of the RGA files remains for future work.

QCM measurements and frequency rates for the unbaked cable are shown in Figure 14. We can make two observations. First, for once we now see a clear difference between the deposition rates on the two QCMs. Both crystals were set to the identical -20 °C set point at the same time, but QCM 1 collects much more mass (higher frequency) by the time the collection ends. This difference indicates that outgassed population does include a substantial component that sticks to the walls and thus does not reach QCM 2. Second, we see also see that the QCM rates are significantly higher than we have seen so far. Around hour 50, which is 4 hours after the start of this test, QCM 1 was collecting at 23,000 Hz/hr, while QCM 2 was collecting at 17,500 Hz/hr. This is a 38 fold increase over the pre-baked flight harness (and a good example why material selection and pre-baking is important). This high outgassing rate limited the time over which the QCM collection could be performed since the QCM crystal generally needs to be baked off once the frequency reaches around 15,000 Hz. Utilizing the average ratio from the four collections between hour 47 and 51, we observe that the rate on QCM 2 is reduced 1.45×. The collection at hour 53 corresponds to the configuration with a cold shroud. In this case, the rate is reduced by a factor of 5.

Figure 15 plots the TGAs collected with this unbaked cable. For the first time, we can now clearly see a difference in populations. In cases (a)-(c), which correspond to the warm shroud, we can observe that the peaks of the QCM 1 population tends to lie around 50 °C, the peak for QCM 2 is located around 32 °C. Interestingly, QCM 1 does not appear to have any peak around this temperature. Analyzing this finding reminds as an action item for future work. Our baseline assumption was that the two populations will be more-or-less identical at the colder temperatures and deviate greatly at temperatures above the wall temperature. This is in fact seen in the subplot (d), which corresponds to the cold chamber wall. Yet even here, the cut off does not happen until about 12 °C, which exceeds the 5 °C recorded chamber shroud temperature.

The corresponding sticking coefficients are visualized in Figure 16. Here we again see that cases (a)-(c) correspond well with each other, with QCM 1 and QCM 2 traces following comparable profiles. The deviation in the green curve for QCM 1 (case d) from the other three traces could be due the electric cord temperature dropping down to 35 °C as the heater could not keep up. The sub unity of c_{stick} at $T < -10$ °C is an artifact

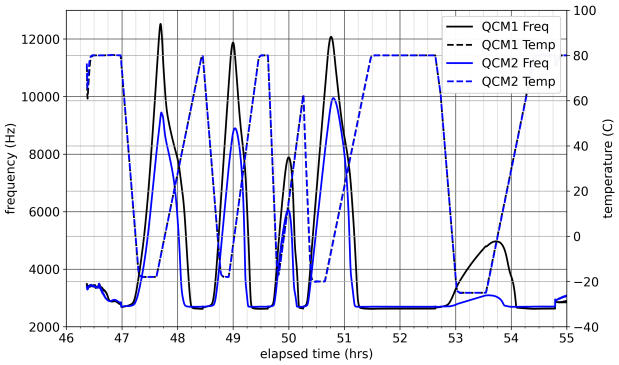

(a) QCM data

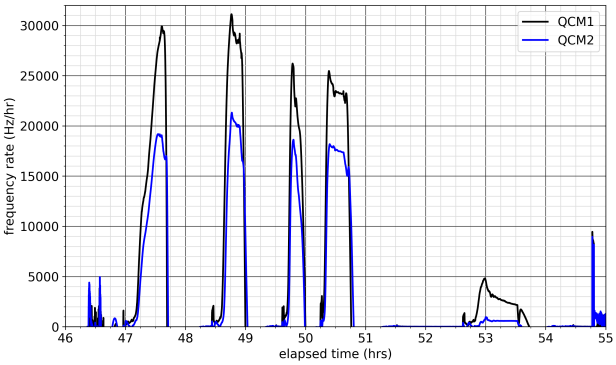

(b) QCM rate

Figure 14. QCM measurements and rates for the unbaked cable.

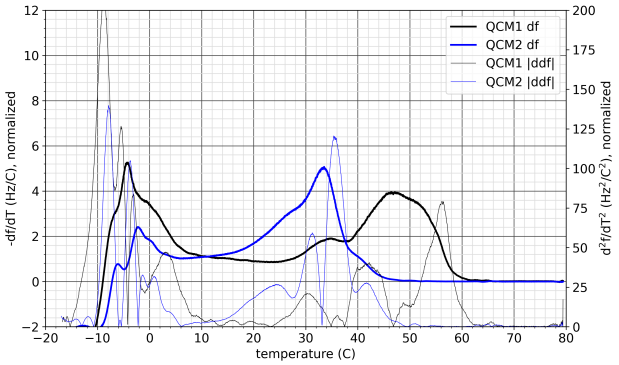

(a) 47.63 to 48.44

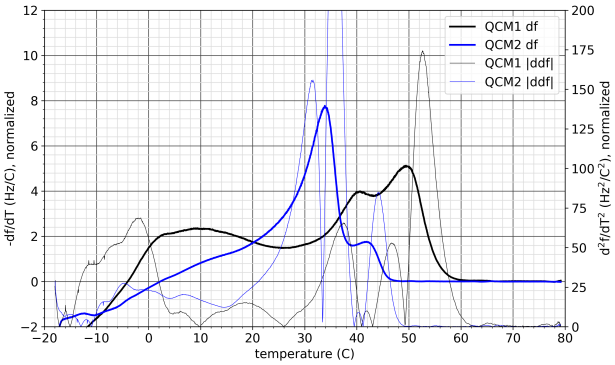

(b) 48.92 to 49.47

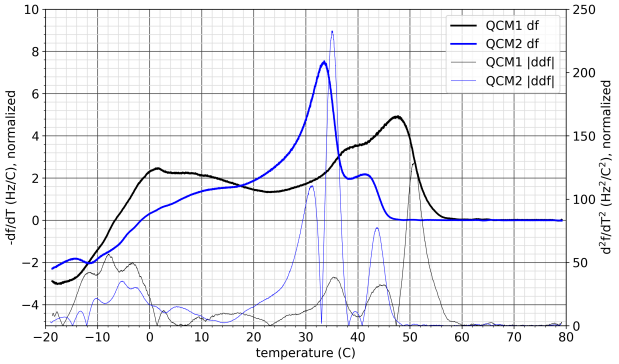

(c) 50.66 to 51.48

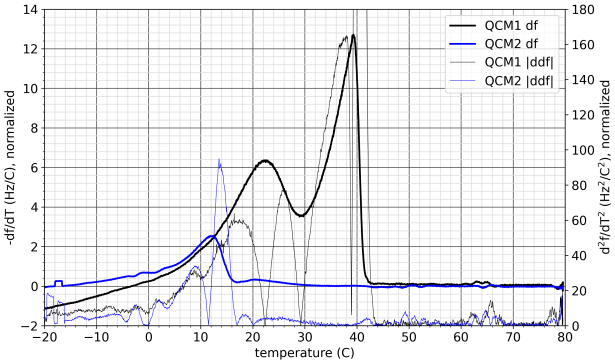

(d) 53.56 to 54.43

Figure 15. TGAs for the unbaked cable.

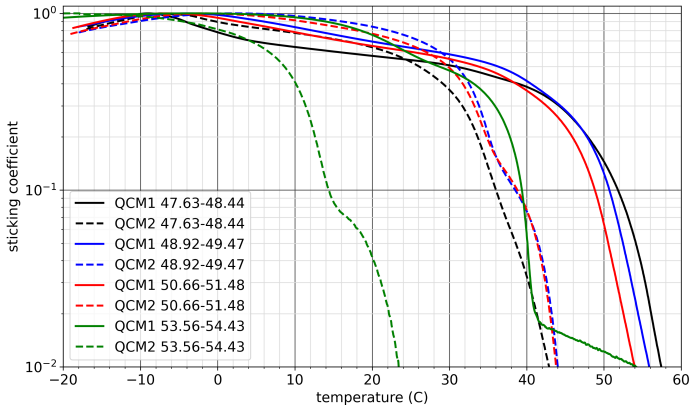

Figure 16. Sticking coefficient for the unbaked cable

of the high outgassing and our normalization. During the TGA, the crystal continues to collect additional mass as long as the temperature is cold enough. This added error is normally negligible, since the newly collected mass is tiny compared to the total amount of mass already deposited on the crystal. That wasn't the case here, however. Due to the high outgassing rate, we were able to collect on the QCM for only about an hour before the crystal had to be baked off. Even at 3 °C/min, it takes over 30 minutes, or half of the collection time, to complete a TGA.

Just as before, the sticking coefficient was extracted and used to run a simulation. The input values were

```
c_stick:[1.0@253.0, 1.0@258.0, 0.98@263.0, 0.97@268.0, 0.90@273.0, 0.82@278.0,
         0.75@283.0, 0.69@288.0, 0.64@293.0, 0.60@298.0, 0.55@303.0, 0.48@308.0,
         0.39@313.0, 0.26@318.0, 0.11@323.0, 0.02@328.0, 0.00@333.0]
```

Results from this simulation are shown in Figure 17. Plot (a) shows the number density with the room-temperature wall, while case (b) corresponds to the colder 5 °C walls from hour 53. Due to some limitation of the surface mesh model, the fixture also had to be set to this cooler temperature (the fixture has not yet been separated into a separate group from the walls). By comparing these two figures, we can notice darker blue shading in the wake behind various structures. This coloring indicates lower density in these regions without a direct line of sight to the source due to the reduce re-emission from the walls. Plot (c) visualizes the time history of the collected masses for these two cases. The case from (b) with the colder walls is shown by the thinner lines. We can see that the colder wall has only a minimal impact on the deposition on QCM 1. This confirms our design assumption that QCM 1 incident flux is mainly driven by line of sight outgassing from the sample. After 200,000 time steps, the mass collected on QCM 1 and 2 is 4.71×10^{-15} and 1.84×10^{-16} for the ambient walls, and 4.46×10^{-15} and 2.29×10^{-17} for the cold walls. In other words, the simulation predicts a 25.6 and 194.8× decrease in deposition rate on the second QCM. While the trend agrees in that we indeed see a higher reduction with the colder walls, the actual decays is over-estimated 17.66× for the warm wall, and 5.12× for the cold wall case. Just as was argued previously, the discrepancy likely arises from the repeated application of the sticking coefficient on subsequent surface impacts.

3.6 Empty Chamber

We also performed another empty chamber baseline measurement at the conclusion of the test to characterize the amount of additional wall contamination introduced by the cable. Chamber telemetry is shown in Figure 18. The first approximately 20 hours were dedicated to sampling outgassing with ambient walls. QCM rates are plotted in Figure 19. Even without a sample present, QCM 1 was recording over 6000 Hz/hr, which is a 43× increase over the baseline in Figure 3. The chamber was thus baked for about 14 hours. This bake out reduced the background 800 Hz/hr, which is still noticeably higher than the 140 Hz/hr observed initially. The TGAs from this characterization are plotted in Figure 20. Running numerical simulations of this configuration, specifically taking into account the impact of bakeout on surface desorption, remains as future work.

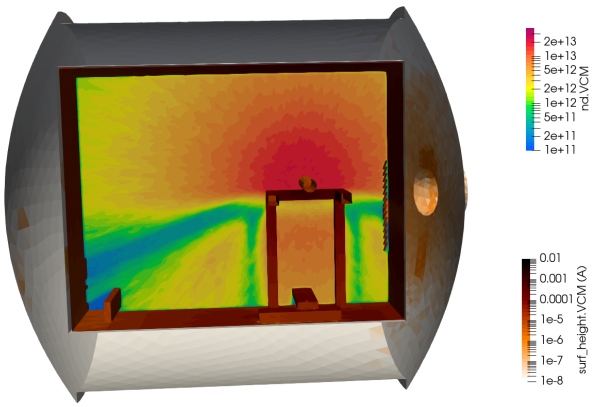

(a) number density, warm walls

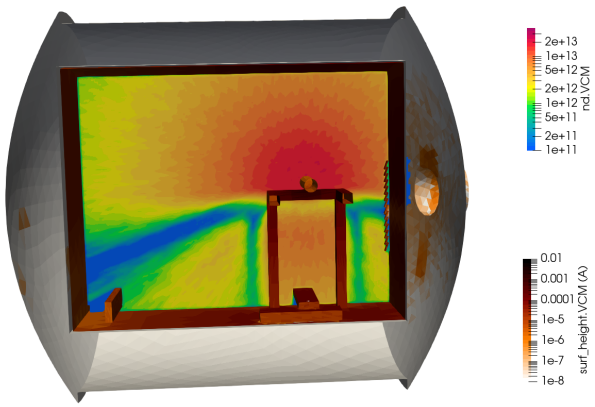

(b) number density, cold walls

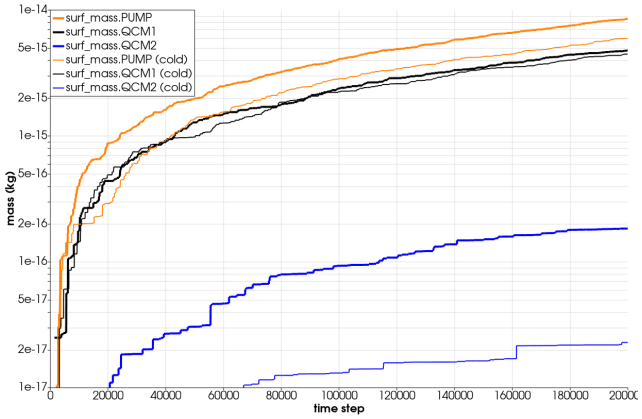

(c) deposited mass

Figure 17. Numerical simulation for the unbaked electrical cable for the warm and cold chamber walls

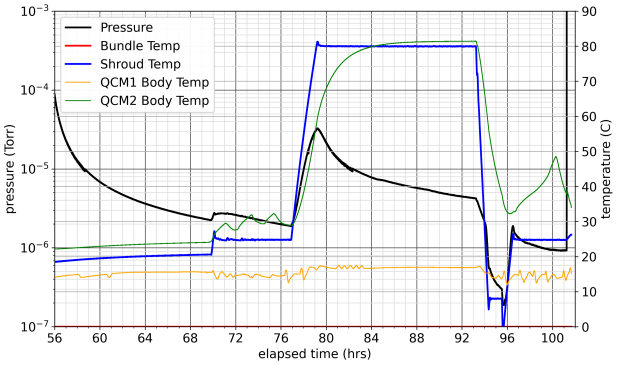

(a) Chamber Telemetry

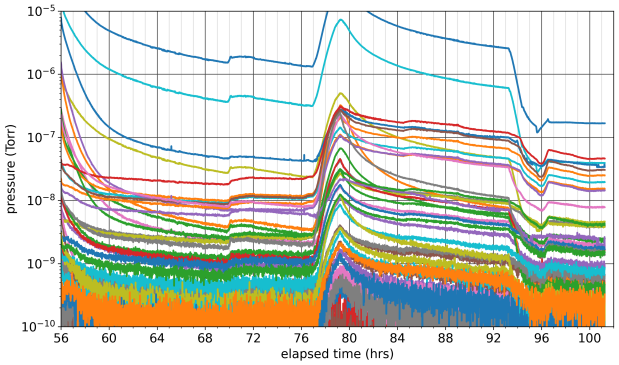

(b) RGA

Figure 18. Empty chamber readouts for a post-test characterization.

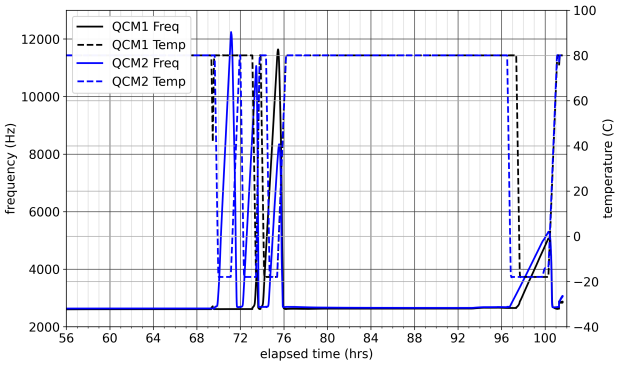

(a) QCM Data

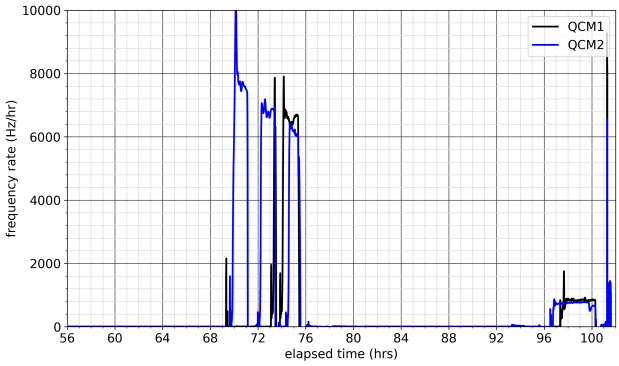

(b) Frequency Rate

Figure 19. QCM data for the empty chamber.

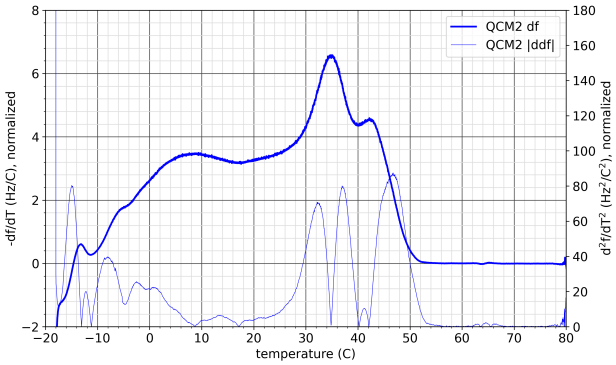

(a) 71.11 to 71.97

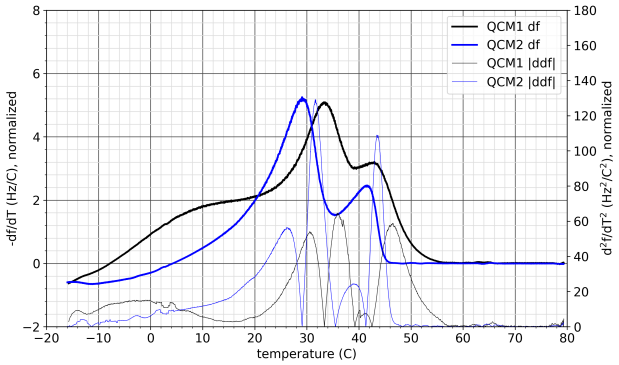

(b) 75.40 to 76.20

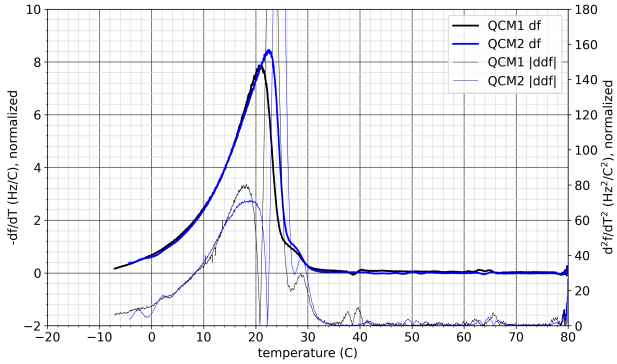

(c) 100.40 to 101.13

Figure 20. TGA for the post-test empty chamber.

4. USC TESTING

We have also conducted a parallel testing campaign using a 40 cm diameter top loaded chamber located at USC's Laboratory for Exploration and Astronautical Physics (LEAP). This chamber is shown in Figure 21. It was originally pumped solely with a single oil-based roughing pump and did not contain any diagnostic equipment. Throughout the performance on this project, the chamber was slowly upgraded. We sourced and integrated a Faraday QCM, a turbomolecular pump, an ion gauge, and a SRS-100 RGA. Most recently, the oil-based diffusion pump was replaced with a dry pump, which helped us eliminate the presence of oil fragments from the RGA

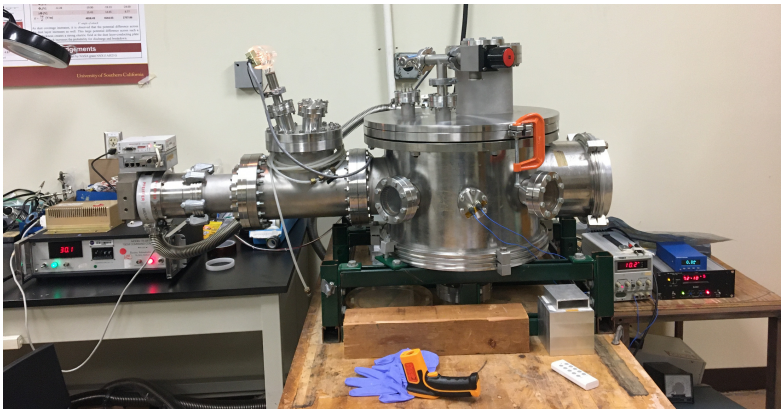

Figure 21. Vacuum chamber used at USC's LEAP lab

spectrum observed in a prior study.[7]

Due to having access to just a single QCM, our experiment was designed to use the same QCM to characterize both the line of sight and the re-emission collection. Specifically, we initially placed the QCM close to, and in the direct view of, of the outgassing sample (Orientation 1). We then repressed the chamber and rotated the QCM to face the chamber wall (Orientation 2). These two orientations can be seen in Figure 22. Here we can also see the copper tape used to provide additional thermal conductive path to cool the QCM body. The Faraday QCM used in this work consists of a large plastic body which reaches warm temperatures while the QCM crystal is maintained cold. Nominally, the QCM should be installed into an actively chilled heat sink, however, this was not possible due to our facility lacking a chiller as well as the appropriate chamber penetration plate. Therefore, we attempted to aid in cooling by adding the copper tape. This configuration also limited the crystal temperature to about -20 °C, however even at this setting, we observed the QCM to begin overheating if left collecting for more than four hours. Since changing the orientation required redoing the tape down, in our later runs we instead moved the sample while keeping the QCM stationary. While we briefly experimented with using several drops of dioctyl phtalate (per recommendation from an external party) placed onto an aluminum foil as an outgassing source, we found this substance difficult to work with due to its high viscosity. Subsequently, we switched to a bundle of electrical connectors as also shown in Figure 22. This bundle was placed onto a heater pad generated by wrapping nickel chromium wire in a Kapton tape. Due to lack of appropriate chamber penetration plates, neither the heater nor the sample could be instrumented with thermocouples. As such, the heater calibration was performed at ambient pressure using a handheld IR thermometer to record temperature as a function of applied power supply voltage. The heater was activated by turning the connect power supply to 9 V, which produced 50 °C temperature at ambient conditions. The chamber walls are not temperature controlled and are roughly equal to room temperature. While the chamber is placed in an air conditioned room, variations in room temperature could be one source of uncertainty in our measurements.

4.1 Baseline

Our prior testing[7] indicated strong presence of roughing pump oil during testing. We could clearly observe the disappearance of various 40 amu and higher peaks on the RGA trace the moment the roughing pump valve was closed. This prior testing also indicated a large baseline outgassing rate in excess of 1500 Hz/hr. Our recent focus was on obtaining an oil-free roughing pump, as we hoped it would eliminate the large baseline. This however has not been found to be the case. After installing the new oil-free pump, the chamber interior was thoroughly wiped with isopropyl alcohol and left under vacuum for multiple days to purge some of the pump oil and other contaminants from the walls. With the new pump, the baseline chamber pressure is 10^{-5} Torr. Multiple baseline measurements were taken with the QCM temperature at -20° C. Measurements consistently showed about 1500 Hz/hr of background contamination from the chamber, which is comparable to what we have seen previously. This baseline is significantly higher than most published standards and what was observed at the Blue Origin chamber. We attempted to heat various components of the chamber externally with an electric heating pad and internally with a segment of bare nickel chromium wire. Neither method proved successful for driving down the

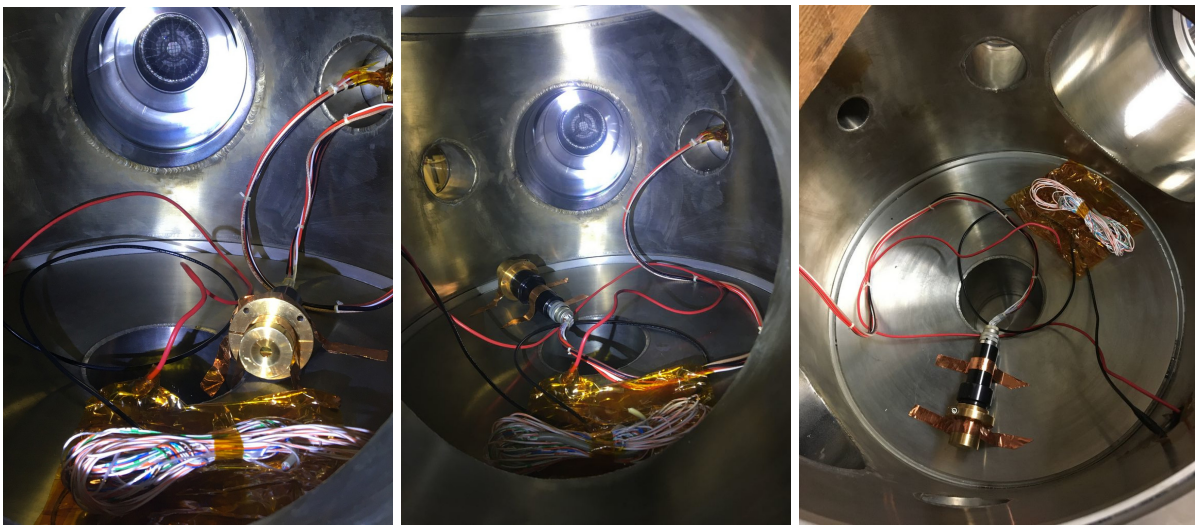

(a) Orientation 1 (b) Orientation 2 (c) Orientation 2, top view

Figure 22. Nominal experimental setup.

background collection rate. We suspect that this high rate may be due to leftover contamination from pump oil and previous experiments, frequent repressing and short collection periods, and the QCM body itself. We were able to see a decrease in rate to about 1100 Hz/hr after leaving the chamber under vacuum with the pumps off over a weekend and running another collection period with the pumps on when we returned. The chamber was then repressed, allowed to sit open for about 10 minutes, and the process was repeated. This resulted in an increase to 1800 Hz/hr. By opening the chamber, we are introducing some unidentified contaminant that is able to collect on the QCM crystal, potentially supporting that our baseline rate is high due to frequent repressing. This contaminant could be arising from other equipment located in the lab, given that the chamber is not located in a dedicated clean room. We were hoping to observe this contaminant on the RGA spectrum, but this was again not the case. With the previous oil-based pump, RGA measurements would show the presence of species greater than 40 amu, as well as more fragmented species below 40 amu. The oil-free pump only gives peaks at 18 amu (water), 28 amu (molecular nitrogen), 32 amu (molecular oxygen), and a small signal at 45 amu (isopropyl alcohol).

4.2 Data Collection

Next, a series of tests was conducted to measure outgassing in both the direct and indirect line of sight orientations. Since changing the orientation required performing a chamber repress, we wanted to confirm the tests are repeatable. Therefore, each test consisted of first collecting QCM rate shortly after the chamber was pumped down to the 10^{-5} Torr pressure. This rate was collected for 30 minutes with the QCM crystal set to -20 °C. The QCM was then shut off for about 45 minutes to cool down. We then performed another 15 minute collection at -20 °C to obtain the second baseline rate. The heater was then activated by turning on the power supply, and this rate was collected for 30 minutes. While the heater activation resulted in an immediate response on the QCM, it did not lead to introduction of individual new species on the RGA spectrum. This behavior is similar to what was observed at Blue Origin. Subsequently,the chamber was repressed, and the wire bundle was moved to a new location (in lieu of moving the QCM). The test sequence was then repeated. Each day, one pair of tests was performed, alternating orientations and repressing in between each so that three total test pairs were conducted. Collection rates for these tests is given in Table 1. RGA measurements were similar to the previous tests with the same species being collected, just at varying partial pressures.

Our hope was that the initial rate will be approximately identical across all six tests, and that the secondary baseline rate, taken 45 minutes later, will also be identical, but lower than the initial rates. However, as can be seen from Table 1, this is clearly not the case. The initial rates vary from 780 Hz/hr to 3120 Hz/hr and

Table 1. Collection Rates for Wire Bundle in Hz/hr

Test Number	Orientation	Initial (Hz/hr)	Secondary (Hz/hr)	Heater (hz/hr)	Increase
1	1	2580	3180	8940	5760
2	1	2220	2580	8700	6120
3	1	2940	3360	8580	5120
1	2	3120	3240	6300	3060
2	2	780	780	2100	1320
3	2	1044	1734	4134	2400

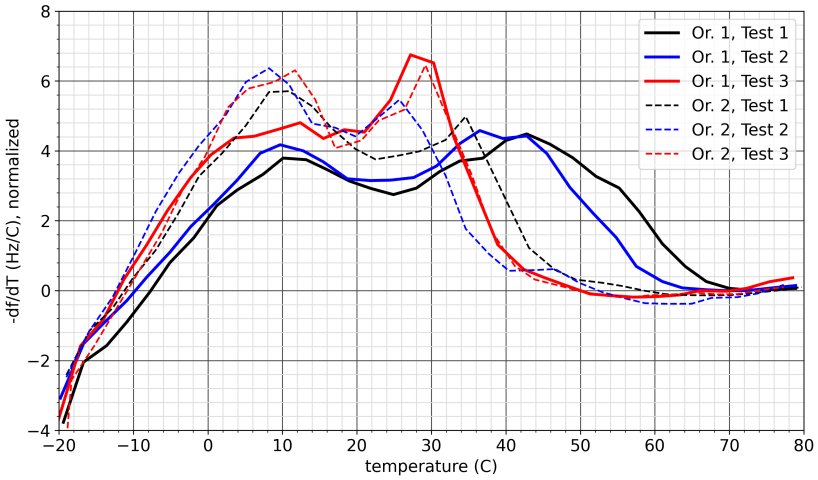

Figure 23. TGA obtained at the USC facility for QCM facing the sample (orientation 1) and QCM facing the wall (orientation 2)

in all cases, the secondary rate is higher, or at least identical, to the initial rate. These measurements clearly indicate the presence of some undetermined outgassing source. They also make interpreting the impact of wall re-emission difficult due to the lack of consistency. While we can clearly notice the increase in outgassing rate once the heater is activated, here we also see a variation. In the direct line of sight orientation 1, the rate increases from 5120 Hz/hr to 6120 Hz/hr, while in orientation 2 it increases from 1320 to 3060 Hz/hr. Averaging these increases, we can estimate that the deposition in Orientation 2 is reduced by a factor of 2.51. However, despite the unpredictable variation in baseline rates, the QTGAs recovered the expected cut off due to wall losses. The TGAs obtained at the end of each of these six tests are shown in Figure 23. The solid lines indicate data from orientation 1, while the dashed lines indicate traces from the wall-facing orientation 2. In all cases, we can see the TGA produce a broad spectrum, without significant individual population. However, the spectrum for orientation 2 is clearly cut off around 40 °C, which similarly to the Blue Origin data, is about 10-15 °C above the wall temperature. The main exception is Orientation 1 Test 2, for which the TGA spectrum is comparable to one obtained with Orientation 2. The source of this discrepancy is not yet understood.

To further investigate the impact of chamber repress on the data, a new test procedure was implemented for one additional set of tests. Instead of repressing the chamber between each test, we now collected a sequence of three outgassing rates in orientation 1, followed by three rates in orientation 2. For each test, we conducted three collection periods. In each collection, the heater was left off for 10 minutes to collect the initial rate and then turned on for 30 minutes. This was followed by a 20 minute cooldown before repeating the collection period two more times. For Orientation 2, a third segment was added to the end of each collection period to observe the new rate after the heater was turned off and allowed to cool for 15 minutes. Only the linear portions of each segment once the temperature of the heater had equilibrated was used. These collections were done with a -5 ° C crystal to minimize QCM overheating. The crystal was also not baked in between each collection to minimize pump heating and QCM overheating, and a TGA was conducted at the end of the three collection periods. Rates for these tests are given in Tables 2 and 3. These tests again produced inconclusive data with

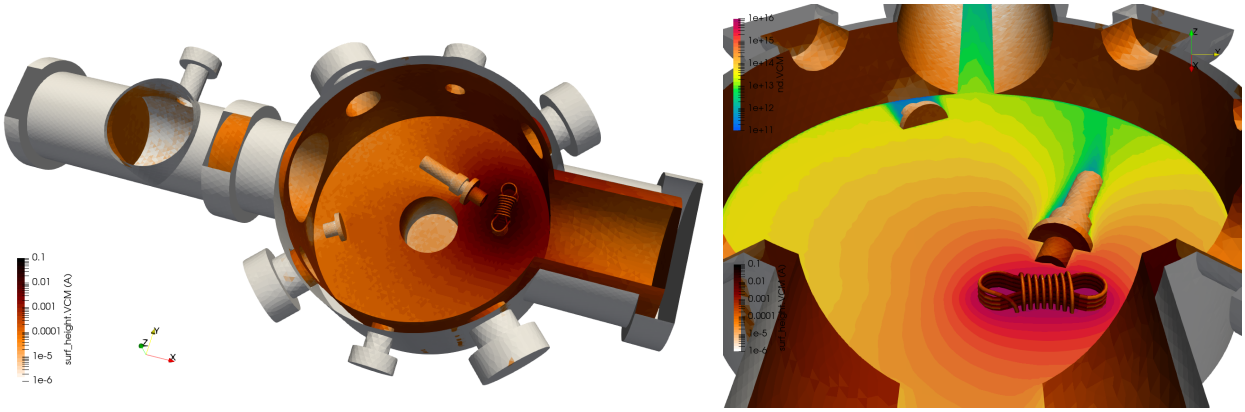

(a) Surface deposition (b) Contaminant number density

Figure 24. Numerical simulation of molecular outgassing in the USC chamber.

the baseline (heater off) rate continuously increasing. The initial baseline rate of 468 and 600 Hz/hr was also noticeably lower than the baseline rates observed in the prior sequence. The ratio between the average increases when the heater is activated is now reduced to 1.67. The variation from the 2.5 value reported above is likely arising from the lower crystal temperature.

Table 2. Collection Rates for Orientation 1 without Repress in Hz/hr

Test	Heater Off (Hz/hr)	Heater On (Hz/hr)	Increase
1	468	2724	2256
2	1140	3480	2340
3	1398	3540	1142

Table 3. Collection Rates for Orientation 2 without Repress in Hz/hr

Test	Heater Off (Hz/hr)	Heater On (Hz/hr)	Heater Cooled (Hz/hr)	Increase
1	600	1740	1560	1140
2	1440	2520	2340	1080
3	2160	3360	3240	1200

The TGA data from tests 1 and 2 in Figure 23 (test 3 was excluded due to being out of family) was used to set the sticking coefficient for a numerical simulation, as shown below.

```
c_stick:[1.00@263.0, 0.99@268.0, 0.96@273.0, 0.90@278.0, 0.82@283.0, 0.73@288.0,
         0.66@293.0, 0.59@298.0, 0.53@303.0, 0.44@308.0, 0.36@313.0, 0.25@318.0,
         0.16@323.0, 0.09@328.0, 0.03@333.0]
```

Results from the simulation run with QCM crystals set to -20 °C are shown in Figure 24. These plots were generated after 200,000 10^{-5} s time steps. The first plot shows the surface deposition thickness for a hypothetical run with two QCMs (with the second one having a smaller footprint). We can clearly see noticeable deposition on the entire chamber, with thickness scaling with the radial distance from the source. This is expected since the derived sticking coefficient data indicates 59% deposition at the 25 °C assumed wall temperature. The second figure visualizes the contaminant number density. While we can see clearly observe shadowing behind the second QCM, the presence of non-zero deposition on the wall, as well as the non-zero contaminant density indicates the presence of gray-body transport. This simulation predicts a 4431× reduction in the deposition rate on the second QCM. Using the 0.59 sticking coefficient value, this reduction corresponds to 15.9 molecular bounces needed to reach the second QCM, which is in line with the finding from the Blue Origin simulations.

Table 4. Summary of experimental and numerical QCM 2 deposition rate reductions

Test	Experimental	Numerical	Error (%)
BO harness	1.0	8.2	720
BO cable, warm wall	1.45	25.6	1666
BO cable, cold wall	5.0	194.8	3796
USC wire bundle	2.51	4431	176433

5. CONCLUSION

This paper described a test campaign designed to experimentally study the feasibility of using QCM-derived temperature based sticking coefficients for modeling gray body molecular transport. The test involved placing a QCM in a direct line of sight of an outgassing sample, and performing a TGA on the collected data to obtain the sticking coefficient. A second QCM was placed facing a chamber wall such that any molecules reaching it had to undergo wall re-emission. We subsequently used the sticking coefficient from the first QCM to run a numerical simulation to predict the reduction of deposition rate onto the second QCM. This numerical result was compared to the experimental data. The testing was performed at Blue Origin's Kent facility and at USC's LEAP lab. While the testing at USC was quite inconclusive due to a yet undetermined source of contamination, both experiments indicate that the QTGA-derived sticking coefficient underestimates the gray-body transmission. The findings are summarized in Table 4. We can observe that the sticking coefficient approach produced average error of 2000% for the flight harness and wire bundle testing at Blue Origin, with a much greater error for the wire bundled tested at USC. The reason for this discrepancy is that the molecular contaminant population is composed of multiple chemical species. Some of these species condense on the first wall impact, while the rest continue bouncing around the chamber unaffected until reaching the colder QCM crystal. The USC testing also suffered from high baseline outgassing and inconsistent rates, which are being investigated.

As part of our future work, we plan to further study the use of QCM-derived data to describe the contaminant behavior. This will involve attempting to map multiple populations of different activation energies to the QCM data. We also plan to continue the experimental campaign at USC by obtaining a new QCM sensor, instrumenting the chamber with thermocouples, and isolating the chamber in a clean enclosure. Data collected at the USC facility is available for download from `https://www.particleincell.com/2022/qcm-coefficients/`. Data collected at Blue Origin is available upon request.

Acknowledgement

The authors would like to acknowledge helpful conversations with John Canham and George Meadows related to QCM operation and outgassing sample selection.

REFERENCES

[1] A. C. Tribble, *Fundamentals of Contamination Control*, vol. 44, SPIE Press, 2000.

[2] L. Brieda, "Numerical model for molecular and particulate contamination transport," *Journal of Spacecraft and Rockets* **56**(2), pp. 485–497, 2019.

[3] L. Brieda and M. Laugharn, "Optimization, development, and validation of the contamination transport simulation code," in *SPIE Optics & Photonics*, 2020.

[4] G. A. Bird and J. Brady, *Molecular gas dynamics and the direct simulation of gas flows*, vol. 5, Clarendon press Oxford, 1994.

[5] C. Birdsall and A. Langdon, *Plasma physics via computer simulation*, Institute of Physics Publishing, 2000.

[6] L. Brieda, M. Laugharn, M. Woronowicz, K. Henderson-Nelson, C. May, and E. Wooldridge, "Numerical study of water ice and molecular contamination build up during JWST deployment," in *SPIE Optics & Photonics*, 2022.

[7] L. Brieda, E. Helou, J. Asher, and J. Wang, "Experimental validation of molecular transport model." NASA Goddard Contamination Control, Materials, and Planetary Protection Workshop, 2021.